Shock Waves (2002) 12: 93–98
Digital Object Identifier (DOI) 10.1007/s00193-002-0147-0

Shock Waves

Hypersonic aerothermodynamic and scramjet research using high enthalpy shock tunnel

K. Itoh, S. Ueda, H. Tanno, T. Komuro, K. Sato

National Aerospace Laboratory, Kakuda, Miyagi 981-1525, Japan

Received 22 July 2001 / Accepted 22 April 2002
Published online 8 July 2002 –

Abstract. A high enthalpy shock tunnel is a potential facility for gaining knowledge to develop modern aerothermodynamic and propulsion technologies. The largest high enthalpy shock tunnel HIEST was built at NAL Kakuda in 1997, aiming for aerothermodynamic tests of Japan's space vehicle HOPE and scramjet propulsion systems. Selected topics from the experimental studies carried out using HIEST so far, such as the nonequilibrium aerodynamics of HOPE, the surface catalytic effect on aerodynamic heating and scramjet performance are described.

Key words: Hypersonic flow, Aerothermodynamics, Scramjets

1 Introduction

To develop modern aerothermodynamic and propulsion technologies for supporting space access and reentry vehicles, the role of hypersonic ground testing at high enthalpy and density conditions is important to gain knowledge on high temperature real gas phenomena. In fact, high enthalpy shock tunnels are the only facilities at present which can generate high enthalpy and density flow so as to duplicate high temperature, real gas effects on aerothermodynamics and combustion under such flight conditions. High enthalpy shock tunnels are distinguished from conventional shock tunnels by their hot driver gas. Thus they can be further classified by the method for heating the driver gas. The most feasible method may be a free piston compression proposed by Stalker (1967), which enables an easy and safe heating of the driver gas to very high temperature. Based on a number of fundamental studies on the characteristic of the free piston shock tunnels, Stalker succeeded in building the T3 (ANU) and T4 (UQ) for high enthalpy flow research until the end of the 1980's. His achievement encouraged the building of larger facilities T5 (CALTECH) (Hornung 1992) and HEG(DLR) (Eitelberg 1994), which are large enough for supporting design efforts, in the early 1990's. The largest facility HIEST was built at NAL Kakuda in 1997 (Itoh et al. 1999), aiming for aerothermodynamic tests of Japan's space vehicle HOPE and also to support scramjet testing. In the present paper, selected topics of aerothermodynamic and scramjet studies with the HIEST are described. The first topic is the result of HOPE aerodynamic testing which was aimed to prove chemical nonequilibrium effects on the aerodynamic characteristics (Itoh et al. 2001). The second topic is the study on surface catalysis which is an important issue concerned with hypervelocity aerodynamic heating (Ueda et al. 2001). Finally, the first campaign of scramjet testing is presented, which was aimed at achieving an impulsive scramjet testing technique and to prove the basic performance of the sub-scale engine (Tanno et al. 2001).

Correspondence to: K. Itoh
(e-mail: itoh@kakuda-splab.go.jp)
An abridged version of this paper was presented at the 23rd Int. Symposium on Shock Waves at Fort Worth, Texas, from July 22 to 27, 2001

2 Facility

The HIEST is a free-piston-driven shock tunnel which consists of a high pressure air reservoir, a compression tube, a shock tube, a nozzle and a test section. The driver gas is compressed adiabatically by the free piston in the compression tube to generate a strong shock wave in the shock tube, so that a high-enthalpy stagnation condition of the test gas can be obtained behind the reflected shock wave at the shock tube end. The HIEST was designed to fulfill the requirements for aerothermodynamic tests at hypervelocity conditions of 3–7 km/s along the HOPE reentry flight and scramjet tests at Mach 8–16 flight conditions at dynamic pressures of 50–100 kPa. The compression tube is 16 m long and 600 mm in diameter, and the shock tube is 17 m long and 180 mm in diameter. In order to achieve the tuned piston operation in the whole range of stagnation enthalpy and pressure required for the tests, five pistons of 220, 290, 440, 580 and 780 kg were made. For aerodynamic tests, a conical nozzle with a throat diameter from 24 to 50 mm and an exit diameter of 1200 mm is used, allowing testing with HOPE models with spans as large

Fig. 1. Overall view of the HIEST

as 500 mm. For scramjet tests, a contoured nozzle with throat and exit diameters of 50 and 800 mm respectively are used. The maximum stagnation enthalpy and pressure are 25 MJ/kg and 150 MPa, respectively. The test duration is 2 ms at the highest enthalpy condition, with a longer time at lower enthalpy conditions.

3 HOPE aerodynamic study

Since the chemical nonequilibrium effect is more severe for a small vehicle such as the HOPE, more accurate knowledge of chemical nonequilibrium aerodynamics is required for design and flight. In the present study, the nonequilibrium effect of oxygen dissociation was intensively investigated by force measurements in the HIEST. The present results are compared with the HOPE reference model based on nonequilibrium CFD results using a two temperature model.

3.1 Experiment

The tests were conducted at stagnation enthalpies from 8 to 24 MJ/kg in which oxygen dissociation likely dominates the nonequilibrium aerodynamic characteristics. The reservoir pressure was fixed at 40 MPa for all test condition, so that the experimental binary scaling parameter was adjusted to the value of the flight at 17 MJ/kg with a nozzle area ratio of 900 and a 2.5% test model of 400 mm in fuselage length. The forces and pitching moment were measured by a force balance with aid of acceleration compensation for the low frequency vibrations of the bending motion of the sting and the pitching motion of the model.

Fig. 2. 2.5% HOPE model equipped with force balance

3.2 Results and discussion

In the HIEST tests, the flow established at 1 to 2 ms after its onset and a stable period of 1 to 4 ms followed. A test window of 0.5 ms was chosen in the middle of the stable period after flow establishment. The aerodynamic coefficients were estimated by averaging the forces and the pitching moment. Since the nonequilibrium effect is less important on the axial force, only the normal force and the pitching moment are discussed here. Figures 3 and 4 show the trends of the normal force coefficient C_N and the pitching moment coefficient C_m on the stagnation enthalpy, compared with the respective values for the HOPE reference, the latter being based on hypersonic wind tunnel tests and nonequilibrium CFD results. It can be noted that the dissociation rate of nitrogen is much smaller than that of oxygen and almost no dissociation of nitrogen occurs except at the nose region. Therefore the nonequilibrium effect with oxygen dissociation is mainly considered here. On the main part of the body and wing, except for the subsonic region at the nose, the pressure decreases with oxygen dissociation, so that the real-gas C_N is generally smaller than the perfect-gas C_N. The maximum decrease in pressure with full oxygen dissociation is estimated to be 7% for this particular shape and attitude of the model. Accordingly, the C_N decrease due to oxygen dissociation may be roughly estimated to be 2–5%. A reasonable decrease could be observed in the HIEST's C_N, as scattered from 1.15 to 1.10, whereas the perfect gas value is 1.18. On the other hand, the reason for the underestimate of the C_N decrease from the nonequilibrium CFD results is not yet known.

Regarding the pitching moment, both the increase in nose pressure and the decrease in fuselage pressure can increase C_m. The decrease in fuselage pressure represents the nonequilibrium effect by dissociation, as the pressure keeps decreasing over the fuselage with the progress of dissociation at a certain rate to the flow speed. Thus, it is expected that the C_m increase with the negative pressure gradient reaches a maximum when the nonequilibrium effect becomes most severe. On the other hand, C_m

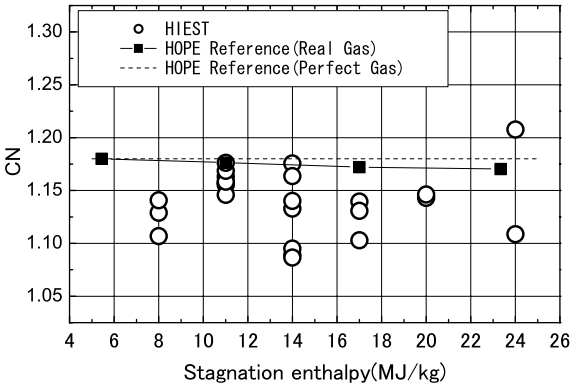

Fig. 3. Normal force coefficient to stagnation enthalpy

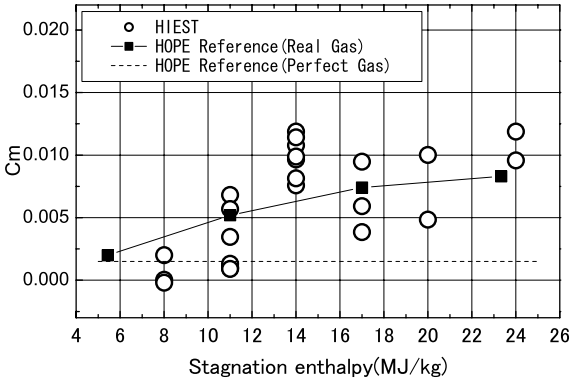

Fig. 4. Pitching moment coefficient to stagnation enthalpy

increases with the nose pressure increase monotonically with the stagnation enthalpy, regardless of whether the chemical state is in nonequilibrium or equilibrium. The HIEST's result seemed to contain both factors for the C_m increase; there was a basic increasing trend with stagnation enthalpy, additionally the peak occurs at around 14 MJ/kg (Fig. 4). The presence of the peak value at around 14M J/kg is possibly correlated with the nonequilibrium effect by considering the ratio of the flow characteristic time and the relaxation time of oxygen dissociation Ω. It is noted that the flow is chemically frozen at $\Omega = 0$, in chemical equilibrium at $\Omega = \infty$ and typical nonequilibrium at $\Omega \sim \mathrm{O}(1)$. The simplified shock layer analysis predicted that C_m reaches maximum at $\Omega = 3.5$ under the present test conditions, whereas the HIEST's C_m reached maximum at around $\Omega = 5.0$. Hence, the experimental and the theoretical values of Ω for the maximum C_m are fairly close and the presence of the peak in the HIEST's result is possibly correlated with the nonequilibrium effect. It may be concluded from the HIEST's results that the chemical nonequilibrium effect with oxygen dissociation appears mostly at moderate or high enthalpy condition. However, the free stream in the HIEST contains unrecombined oxygen atoms due to the nonequilibrium nozzle flow (estimated mole fraction is 0.06 at 14 MJ/kg and more at higher enthalpy conditions), which was not considered in the CFD. The influence of the unrecombined oxygen atoms on the nonequilibrium aerodynamic characteristics is an ongoing study.

4 Surface catalysis study

In atmospheric reentry flight where the aerodynamic heating becomes most severe, a significant amount of the energy of high temperature gas around the vehicle is spent to excite the internal state of the molecules resulting in the dissociation. Therefore, use of a low catalytic material for the thermal protection of the vehicle, such as a SiO_2-based material, is effective in minimizing the aerodynamic heating. The characteristics of low catalytic materials have been intensively studied in different places around the world. From experiences of ground and flight tests, it has been suspected that surface catalysis may strongly depend on changes in surface temperature and density. But the detailed characterization of surface catalyticity is still inadequate, mainly due to the lack of experimental data at sufficiently high density equivalent to flight conditions, since ground tests have been conducted only in low-density facilities such as arc-heated wind tunnels and plasma wind tunnels. The only capable facility of duplicating high-density flow may be a high-enthalpy shock tunnel. However, the short test duration of the high enthalpy shock tunnel is a severe drawback, because the surface temperature of the test model increases only a few degrees from room temperature, whereas the critical temperature range for the surface catalysis change is thought to be 500 to 1000 K. In the present study, a challenging attempt was made on adjusting the surface temperature of the model to a sufficiently high temperature required for catalysis change by installing a pre-heating system in the model.

4.1 Experiments

The tests model is a 373 mm long and 260 mm wide flat plate with a blunt nose, as shown in Fig. 5. There are two reasons for choice of the flat plate model. First, the pressure on the flat plate in the shock tunnel test is generally adjustable to the nose pressure at flight conditions, whereas the stagnation pressure of the shock tunnel may be too high. Secondly, diaphragm fragments often hit and damage the nose so that the catalytic effect may be affected significantly. A blunt nose may withstand such impacts better. Silicon dioxide was coated on half of the flat plate as the low catalytic material and Ag was coated on the other half as the reference high catalytic material. On both sides, 10 thermocouples were mounted in line. Heat fluxes were measured from the temperature changes recorded on the thermocouples. The surface catalytic effect was estimated by comparing the heat fluxes of SiO_2 coating with those of Ag coating or with CFD results. Heaters were installed in the model and adjusted the surface temperature from 300 to 1000 K. It was expected that the pre-heating would change the catalytic reaction rate k_w from O(0.01) to O(1) with which the heat flux would

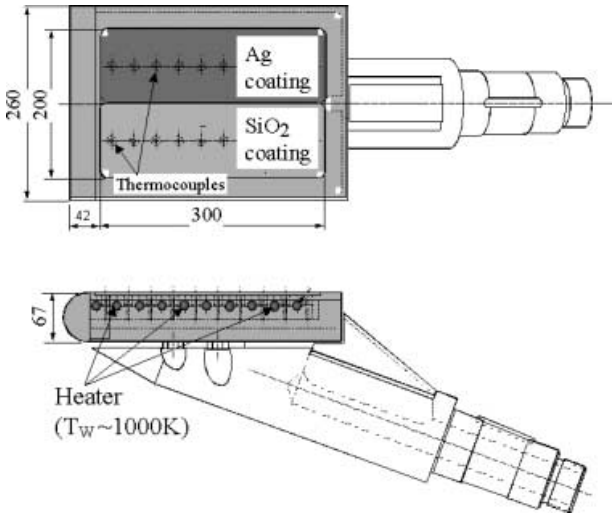

Fig. 5. Flat plate catalytic model with SiO_2 and Ag coating

be changed from a nearly non-catalytic to a full-catalytic value.

4.2 Results and discussion

The tests were carried out at 14 MJ/kg and 20 MPa in stagnation enthalpy and pressure, respectively, with a contoured nozzle of area ratio 256. From CFD analysis, it could be expected that most of the oxygen molecules were dissociated in the high recovery temperature region near the wall and the increment in heat flux with the recombination by wall catalysis was estimated to be 40% of total heat flux. Figure 6 shows the heat flux distributions on SiO_2 and Ag coatings along the model for surface temperatures of 290 and 420 K. The heat fluxes of SiO_2 were equivalent to the non-catalytic CFD result as expected due to its small k_w at 290 K. The silver coated heat fluxes were larger than those of the SiO2 coat. The effect of the difference in wall catalysis between Ag and SiO_2 is clearly shown. But the silver-coated heat fluxes were slightly smaller than the full catalytic CFD result in spite of its large k_w value. The reason for this discrepancy is not known yet. In the case of a surface temperature of 420 K, the SiO_2-coated heat fluxes were significantly increased from the room temperature result, whereas silver-coated heat fluxes did not change. These changes in the SiO_2-coated heat fluxes with surface temperature were probably caused by the change in k_w. The experiments were conducted at the surface temperature of up to 800 K and the results are also shown in Fig. 7. Each SiO2's heat flux was normalized by the fully catalytic CFD results and they were averaged over the flat plate and plotted to the inverse of surface temperature in Fig. 7. Strong temperature dependence of surface catalysis was observed from room temperature to 570 K, as the normalized SiO_2-coated heat flux increased with surface temperature. It is remarkable that the temperature dependence of surface catalysis appears at a relatively lower temperature in the present tests than those in data obtained in lower density wind tunnel tests, i.e., at 400–800 K. This early appearance of the temperature dependence of surface catalysis may be associated with a high density effect which is expected to be resolved by the high enthalpy shock tunnel tests.

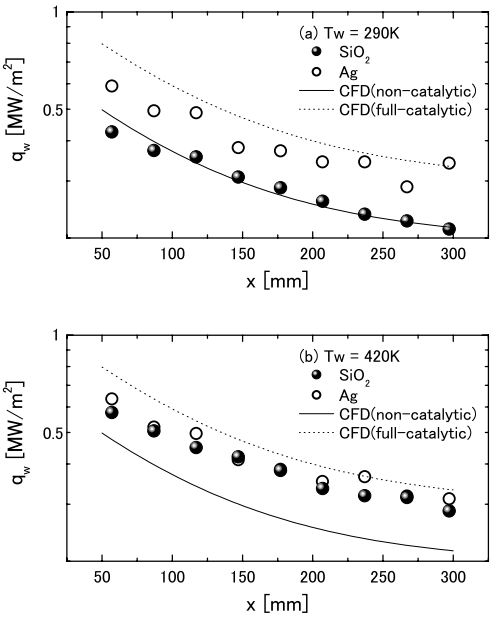

Fig. 6. Heat flux distribution on the flat plate model for surface temperatures of 290 and 420 K

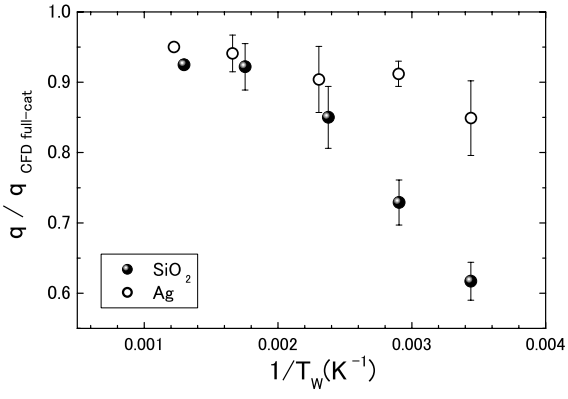

Fig. 7. Temperature dependence of SiO_2 heat flux averaged over the plate

5 Scramjet study

The scramjet engine is a key potential propulsion technology for space access and is expected to generate thrust at Mach 4 to 15. As this kind of airbreathing engine is designed to work at sufficiently high dynamic pressure, i.e., 50 to 100 kPa, the high enthalpy shock tunnel is the only possible existing class of facilities for scramjet ground testing at the higher Mach numbers within the flight envelope. There are several issues concerned with the short duration time of a shock tunnel, such as fuel injection, stability of flow and combustion phenomena, and force measurement.

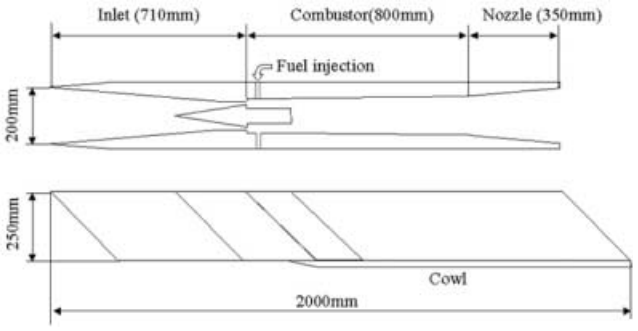

Fig. 8. Scramjet engine model

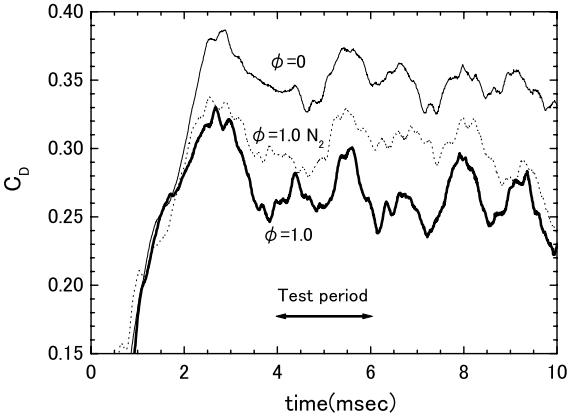

Fig. 9. Time resolved drag coefficients for $\phi = 0$ and 1 at Mach 8

Mixing of fuel and air and combustion reaction are particular issues concerned with the stability of phenomena in a shock tunnel test. The air/fuel mixing process was successfully observed by an advanced planar laser-induced fluorescence technique at T3 and it was found that the mixing became stable very quickly, i.e., within 1 ms for a combustor of several tens of cm long. Regarding the time required for the combustion reaction, an ignition time is thought to be the most critical and it is estimated to be sufficiently short compared to the duration of the high enthalpy shock tunnel. The stability of combustion reaction was well confirmed at T3 and T4. These results of the stability of the phenomena are available for the HIEST tests by simple scaling of the sizes of the facility and model. However, the matters of fuel injection and force measurement are more severe for the larger facility, as larger mass flow rates and total amount of fuel are injected and a heavier model is used. New fuel injection and force measurement techniques have been developed to enable scramjet testing. In this section the outline of the first campaign of the scramjet tests with HIEST is described.

5.1 Experiments

The scramjet engine model tested in the present study consists of the inlet, isolator, combustor, diverging nozzle and the strut, as shown in Fig. 8. Hydrogen was used as the fuel and it was injected from 12 orifices on both sidewalls in the combustor. The engine was equipped with 13 accelerometers as well as 41 pressure transducers. The forces could be estimated from the accelerations, as the engine was suspended by very thin wires and could move freely. The tests were conducted at stagnation enthalpies of 3.3–7.5 MJ/kg, which correspond to Mach 7–13 flight conditions. The stagnation pressure was maintained at 14 MPa for all tests, so that the dynamic pressure could be adjusted to be 50 kPa for the Mach 8 condition. The Mach 8 condition is the standard condition for the NAL RJTF blowdown facility.

5.2 Results and discussion

First, test results for the basic characteristic of the engine as a function of the the fuel equivalence ratio ϕ is discussed for the Mach 8 condition. Time resolved drag coefficients C_D for the cases of equivalence ratio $\phi = 0.0$ and 1.0 are shown in Fig. 9. In order to distinguish the net effect of the combustion on drag reduction from the recoil effect by fuel injection, a reference test with nitrogen was carried out and the result is also displayed in Fig. 9. In all cases, C_D increased after flow onset and reached a maximum at around 2.5 ms. The maximum values for the cases using air and nitrogen as the test gas at $\phi = 1.0$ are almost the same, whereas the maximum C_D at $\phi = 0.0$ is larger. The difference in maximum values between $\phi = 0$ and 1.0 probably showed the recoil effect by the fuel injection. The drag coefficient decreased as the flow was established in the combustor and diverging nozzle. When the flow was well established, the C_D for the air and nitrogen test gas at $\phi = 1.0$ deviated from each each other significantly, showing the effect of combustion.

The pressure distribution along the centerline on the sidewall, which was estimated for the test window of 4.0–6.0 ms, is shown in Fig. 10. The large pressure rise on the isolator was due to the shock wave generated by the strut. After the drop at the backward facing step, the pressure was increased by the recompression and reflected shock. As the flow expanded when it passed the strut, the pressure dropped again. The pressures for the $\phi = 0.0$ and 1.0 cases are almost the same values upstream of the fuel injector. The pressure for the $\phi = 1.0$ case started to deviate higher slightly downstream of the fuel injector, and significant deviation can be seen downstream of the strut. Therefore, it is thought that combustion took place somewhere within 200 mm from the fuel injector. It is remarked that the pressure difference between $\phi = 0.0$ and 1.0 is consistent with the drag reduction. The tests were conducted at ϕ of up to 2.2 and the thrust increment obtained are compared with that obtained in the RJTF as shown in Fig. 11. The equivalence ratio was limited to a maximum of 2.2 in the present test, due to the operating pressure limit for the present fuel injection system. The thrust increased with ϕ and did not stop increasing even at maximum ϕ, whereas the flow was choked at around $\phi = 1$ in the RJTF. The difference in the results between the HIEST and the RJTF might be due to the presence of thick boundary layer flow

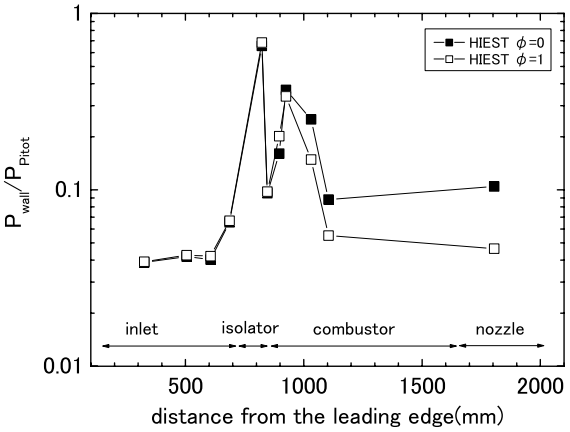

Fig. 10. Pressure distribution on the sidewall for $\phi = 0$ and 1 at Mach 8

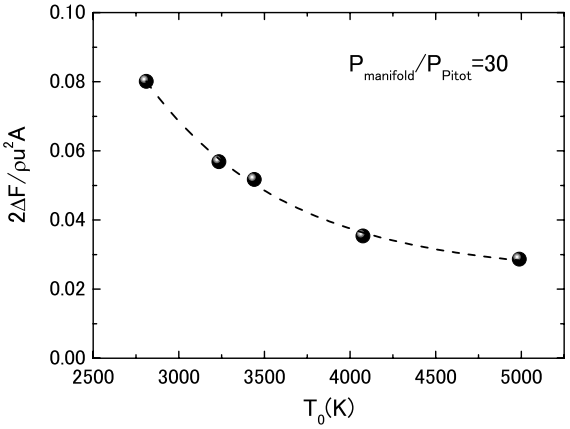

Fig. 12. Change of thrust increment with stagnation temperature

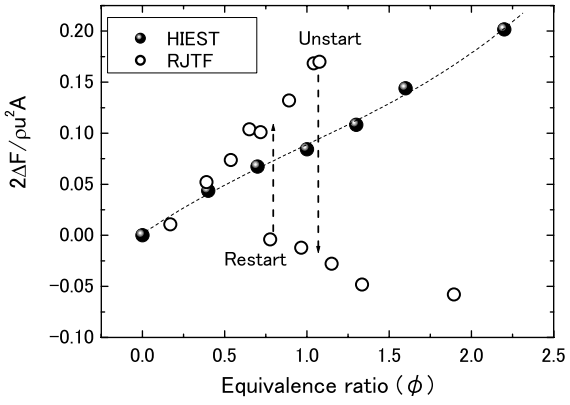

Fig. 11. Thrust increment to ϕ at Mach 8

in the RJTF, whereas the nozzle core flow was used in the HIEST. The increase in the thrust far beyond $\phi = 1.0$ implies that the combustion efficiency of the present engine was not good enough. Since the pressure and temperature in the combustor were estimated to be sufficiently high to ignite the fuel, lower combustion efficiency is thought to be related to the mixing efficiency.

The characteristic of the present engine with respect to the stagnation enthalpy was examined. Figure 12 shows the net effect of the combustion on the drag reduction versus stagnation enthalpy. The net effect of the combustion was estimated by the difference in C_D for the air and nitrogen test gas. As shown in the figure the drag reduction significantly decreased with the stagnation enthalpy. Considering that the ratio of the combustion time and characteristic time of the flow could be estimated to be decreasing with the stagnation enthalpy, it is most likely that the decrease in the drag reduction with stagnation enthalpy is due to the reduction in mixing efficiency.

6 Conclusion

Recent results of aerothermodynamic and scramjet studies with HIEST were reported here. The role of hypersonic ground testing at high enthalpy and density condition was demonstrated. Besides the capability of producing high enthalpy and density flow, the use of a high-enthalpy shock tunnel involves several issues which limit the improvement of accuracy, such as uncertainties due to nozzle throat melting, nonequilibrium thermochemistry in nozzle flow, etc. Intensive attempts are being made on solving the issues throughout the world and it is expected that more accurate data will be provided in the near future.

References

Eitelberg G (1994) First results of calibration and use of the HEG. AIAA 94-2525

Hornung HG (1992) Performance data of the New Free-Piston Shock Tunnel at GALCIT. AIAA 92-3943

Itoh K, Komuro T, Sato K, Tanno H, Ueda S (2001) Hypersonic aerodynamic research of HOPE using high enthalpy shock tunnel. AIAA 01-1842

Itoh K, Ueda S, Komuro T, Sato K, Tanno H, Takahashi M (1999) Hypervelocity Aerothermodynamic and Propulsion Research Using a High Enthalpy Shock Tunnel HIEST. AIAA 99-4960

Stalker RJ (1967) A Study of the Free-Piston Shock Tunnel. AIAA J 5(12): 2160–2165

Tanno H, Komuro T, Sato K, Itoh K, Ueda S (2001) Experimental study on flow establishment in a large scale scramjet. AIAA 01-1889

Ueda S, Komuro T, Sato K, Tanno H, Itoh K (2001) Study on surface catalytic effect using high enthalpy shock tunnel. AIAA 01-1768